



Contents lists available at SciVerse ScienceDirect

Journal of Electromyography and Kinesiology

journal homepage: www.elsevier.com/locate/jelekin

Propagation direction of natural mechanical oscillations in the biceps brachii muscle during voluntary contraction

Akibi A. Archer^{a,*}, Perry Atangcho^b, Karim G. Sabra^a, Minoru Shinohara^{c,1}

^a Woodruff School of Mechanical Engineering, Georgia Institute of Technology, Atlanta, GA 30332, USA

^b School of Biomedical Engineering, Georgia Institute of Technology, Atlanta, GA 30332, USA

^c School of Applied Physiology, Georgia Institute of Technology, Atlanta, GA 30332, USA

ARTICLE INFO

Article history:

Received 14 June 2011

Received in revised form 9 September 2011

Accepted 22 September 2011

Available online xxx

Keywords:

Mechanomyogram

Coherence

Biceps brachii

Vibration

ABSTRACT

The aim of the study was to determine the directionality of the coupling of mechanical vibrations across the biceps brachii muscle at different frequencies of interest during voluntary contraction. The vibrations that are naturally generated by skeletal muscles were recorded by a two-dimensional array of skin mounted accelerometers over the biceps brachii muscle (surface mechanomyogram, S-MMG) during voluntary isometric contractions in ten healthy young men. As a measure of the similarity of vibration between a given pair of accelerometers, the spatial coherence of S-MMG at low ($f < 25$ Hz) and high ($f > 25$ Hz) frequency bands were investigated to determine if the coupling of the natural mechanical vibrations were due to the different physiological muscle activity at low and high frequencies. In both frequency bands, spatial coherence values for sensor pairs aligned longitudinally along the proximal to distal ends of the biceps were significantly higher compared with those for the sensor pairs oriented perpendicular to the muscle fibers. This difference was more evident at the higher frequency band. The findings indicated that coherent mechanical oscillations mainly propagated along the longitudinal direction of the biceps brachii muscle fibers at high frequencies ($f > 25$ Hz).

Published by Elsevier Ltd.

1. Introduction

Continuous surface mechanical oscillations are naturally generated by skeletal muscle during voluntary contraction. These natural muscle vibrations result from the dimensional changes in muscle fibers and muscle-tendon geometry (Beck et al., 2005; Orizio, 1993). Independent of the type of sensors used, recordings of muscle mechanical oscillations with these sensors are called surface mechanomyograms (S-MMGs) (Orizio, 1993).

The physiological origin and time-frequency characteristics of S-MMGs depend on muscle structure, mechanical state, and the electromechanical coupling efficiency in muscles (Barry and Cole, 1990; Oster and Jaffe, 1980; Shinohara and Søgaard, 2006). S-MMGs have typically been used to monitor the mechanical activity of a contracting muscle. In contrast, S-MMGs have rarely been used to estimate the mechanical properties (e.g. viscoelasticity) of skeletal muscles (Cole and Barry, 1994). Indeed, since the S-MMGs correspond physically to propagating vibrations along the muscle, Sabra and his colleagues Sabra et al. (2007) and Sabra and Archer (2009) have been exploring the use of S-MMGs as a potential tool

for non-invasive examination of muscle viscoelastic properties, such as muscle stiffness.

Despite the large body of literature on S-MMGs, the spatial variations of S-MMGs over a muscle remain unclear, specifically the frequency dependency of the spatial variation of S-MMGs. Most studies have used only a single sensor, and the influence of the sensor location over the muscle of interest was investigated only recently from various perspectives (Ouamer et al., 1999; Cescon et al., 2004, 2007, 2008; Madeleine et al., 2006, 2007; Farina et al., 2008). In particular, studies using a two dimensional array of accelerometers have shown that the S-MMGs' amplitude and frequency content is strongly influenced by the sensor location over the studied muscles (Sabra and Archer, 2009; Madeleine et al., 2007; Farina et al., 2008; Cescon et al., 2008). In these studies, the S-MMG analysis was predominantly on low-frequency content (i.e., mainly $f < 25$ Hz) that appeared to be mostly influenced by global synchronized activity of muscle fibers due to tremor activity or electrical stimulation. In preliminary studies using a single subject, high-frequency S-MMGs (i.e., filtered > 25 Hz) of the biceps brachii and vastus lateralis muscles mainly propagated longitudinally along the muscle fiber orientation during sustained voluntary contractions (Sabra et al., 2007; Sabra and Archer, 2009). Indeed these high-frequency S-MMGs were likely generated by asynchronous muscle fiber activity for these superficial muscles and were likely not significantly influenced by synchronized tre-

* Corresponding author.

E-mail address: aarcher6@mail.gatech.edu (A.A. Archer).

¹ Minoru Shinohara is supported in part by VA MERIT Pilot Award (1 I01 RX000421-01).

mor activity that occurs at lower frequencies. No studies are found in the existing literature that systematically investigated directionality of the coupling of the measured S-MMG between low and high frequency bands.

For a given pair of vibration sensors (here skin-mounted accelerometers), the spatial coherence of the S-MMGs is a measure of the similarity of the S-MMGs measured at those two sensors (Gardner, 1992). For instance, the spatial coherence of mechanical vibrations increases when these vibrations propagate along a more homogeneous (or uniform) medium such that the relative phase of the propagating vibration signals remains relatively undisturbed. The main aim of this study was to systematically determine the directionality in different frequency bands of the spatial coherence of the S-MMGs from the biceps brachii muscle during submaximal isometric voluntary contractions using a two-dimensional array of skin-mounted accelerometers (see Fig. 1). Preliminary studies that investigated the directionality of natural muscle vibrations in one subject did not study the influence of the selected frequency band of the S-MMG (Sabra et al., 2007; Sabra and Archer, 2009). The spatial variation of S-MMG coherence across all sensor pairs at low ($f < 25$ Hz) and high ($f > 25$ Hz) frequency bands can then be used to infer how the S-MMG coherence varies with directionality (i.e., longitudinal vs. transverse) and sensor separation distance for various contraction levels.

In this work, the longitudinal direction corresponds to the main orientation of the biceps brachii muscle's fibers and is expected to be more homogeneous than the transverse directions (Fung, 1988). The high frequency mechanical oscillations ($f > 25$ Hz) are less influenced by synchronous tremor-like activity (Orizio, 2005). Therefore, the high frequency oscillations are more likely to propagate coherently along the muscle fiber orientation (i.e., longitudinal direction) similarly to elastic guided waves propagating along cable (or fiber) bundles (Romano et al., 2005). Consequently, it was hypothesized that the spatial coherence of high frequency S-MMG ($f > 25$ Hz) is overall higher in longitudinal directionality (i.e., along the muscle axis) than in transverse directionality (i.e., across muscle fibers).

2. Methods

2.1. Subjects

Ten healthy and right-handed men (age: 29 ± 5 years, height: 175 ± 9 cm, body mass: 71 ± 8 kg), with no overt sign of neuromuscular diseases, volunteered to participate in the present study and signed an informed consent form. This study was conducted according to the protocol approved by the Institutional Review Board of the Georgia Institute of Technology. For each subject,

the thickness of the skin and fat layer overlaying the belly of the biceps brachii muscle was measured to be 2.7 ± 0.8 mm from conventional ultrasound B-mode images (GE LOGIQ P5, GE Healthcare, Waukesha, WI).

2.2. Experimental setup

Fifteen miniature single-axis accelerometers (A352C65, mass = 2 g, base diameter = 9.5 mm, measurement range = ± 491 m/s² pk (50 g pk), sensitivity = 100 mV/g; PCB Piezotronics, Depew, NY) with thin flexible cables to reduce drag (< 1 mm diameter) were used to record S-MMG over the biceps muscle (Fig. 1). The accelerometers were skin-mounted over the biceps brachii using double-sided medical tape to provide good contact while minimizing mounting artifacts and allowing the muscle to move freely without additional pressure interference. Previous studies have demonstrated that a mass up to 30 g on the skin does not significantly affect the S-MMGs' physical characteristics in large skeletal muscles (Cescon et al., 2002; Watakabe et al., 2003).

The accelerometers were arranged on a 3×5 grid (Fig. 1(b,c)). The biceps brachii length was determined based on anatomical landmarks for each subject as extending from the origin of the tendon of insertion (distally) to the coracoid process of the scapula (proximally) Graaff (2002). The sensor grid axis and thus imaging plane was approximately aligned with the longitudinal axis of the biceps brachii. This longitudinal axis corresponds to the muscle fiber orientation since the biceps muscle has a simple fusiform architecture (Pappas et al., 2002). The transverse sensor spacing along the medial-lateral direction (Δx) was set to 2 cm. This distance was the smallest achievable separation distance given the sensor diameter of ~ 9.5 mm. The longitudinal spacing distance along the proximal-distal direction between adjacent accelerometers (Δy) was determined as 8% of the estimated length of the biceps brachii long head muscle ($26 \text{ cm} < L_m < 34 \text{ cm}$), following a previous approach (Sabra and Archer, 2009; Pappas et al., 2002). In this study, Δy varied from 2.1 cm to 2.7 cm among subjects to ensure that the accelerometers were placed in anatomically comparable positions for each subject. Consequently for all subjects, the 3×5 sensor grid covered the region between 18% and 50% of L_m , where the coordinate origin was set at the distal end (0% of L_m) (Pappas et al., 2002).

2.3. Experimental protocol

For each subject, the S-MMGs were recorded during 10 s long voluntary isometric contractions with elbow flexors. A dynamometer (HUMAC, CSMi Medical Solutions, Stoughton, MA) was used as a platform for muscle contraction. Each subject was situated laying on his back with the right arm attached to the dynamometer at the wrist (Fig. 1(a)). The elbow was flexed at 90 degrees, and the wrist was oriented in the neutral position. The right upper arm was placed horizontally with its posterior part not touching the bed surface. A supporting stand for sensor cables was used to minimize motion/deformation artifacts during contractions. The rotation axis of the elbow joint was visually aligned with the rotation axis of the dynamometer. The force output of the biceps was recorded independently by a force transducer attached to the horizontal bar connected to the subject's wrist by a velcro strap. The cables of the five accelerometers located on each of the three longitudinal grid lines (e.g., lateral grid line sensors 1–5, see Fig. 1(c)) were firmly attached with an equal cable length to one of three plywood boards. The boards extended from a sturdy vertical platform that was separated and insulated from the potential vibrations generated by the dynamometer bench. The three plywood boards were stacked vertically to prevent the wires from contacting with each other (see Fig. 1(a)). Each stack board was extended horizontally

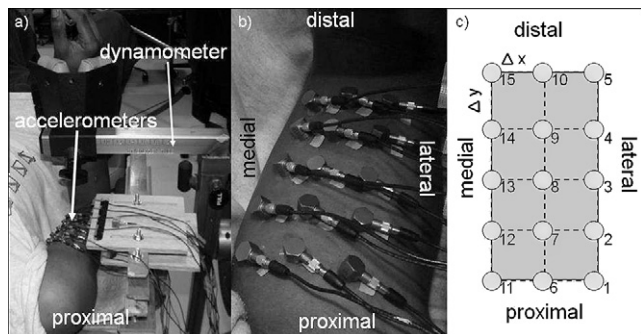


Fig. 1. (a) Experimental set-up for isometric elbow flexion tests, (b) top view of one subject's right arm with the 15 skin-mounted accelerometers, (c) schematic of the 15 accelerometers locations.

so that the cables from adjacent longitudinal sensor lines did not touch. A preliminary study, using the magnitude squared coherence technique described in 2.5, found no significant vibration coupling (i.e., crosstalk) between a reference accelerometer attached to the plywood board and the skin-mounted accelerometers on the biceps brachii muscle of the tested subject.

The maximal voluntary contraction (MVC) force for each subject was determined based on the maximum force output measured over 3 maximal voluntary contractions. Thereafter, subjects performed sub-maximal isometric contractions, in which they were asked to produce and maintain 20%, 40%, and 60% of MVC force for 10 s while facing a video monitor displaying force output as visual feedback. Subjects were encouraged to rest and relax for 3 min between each contraction in order to minimize artifacts due to muscular fatigue. A total of three trials were performed, where one trial consisted of a randomized order of contraction levels (20%, 40% and 60%).

2.4. Data preprocessing

All 15 channels for the recording of S-MMGs were time synchronized with a sampling frequency of 1 kHz (Compact DAQ system, National Instrument®, Austin, TX) and were amplified with a gain of 200. Data were filtered in the frequency band ($f_1 = 5$ Hz and $f_2 = 250$ Hz), using a second order Butterworth bandpass filter. The lower frequency bound f_1 was selected in order to remove the lowest frequency oscillations in order to reduce the eventual bias resulting from motion artifacts (e.g., due to large movements of the whole limb) (Brown et al., 1982; Goldenberg et al., 1991). The upper frequency bound f_2 was set to 250 Hz, the frequency at which no significant S-MMG signal was recorded above the noise floor (e.g., see Fig. 2(a)). The mean power frequency (f_{MP}) of the recorded signal was defined as:

$$f_{MP} = \frac{\int_{f_1}^{f_2} f G_{II}(f) df}{\int_{f_1}^{f_2} G_{II}(f) df} \quad (1)$$

where $G_{II}(f)$ is the power spectrum of the signal $l(t)$ (Kwatny et al., 1970).

The Signal-to-Noise Ratio (SNR) was defined as the ratio of the power of the S-MMG recorded during submaximal contractions to the power of the S-MMG measured at the baseline (0% MVC). For each S-MMG, the power was computed in the same frequency band [$f_1 = 5$ Hz - $f_2 = 250$ Hz]. The values for the 15 accelerometers and 3 trials were averaged and realized as one value for each subject. The mean (and SD) were then found across the ten subjects giving $n = 10$ (subjects) for the SNR and f_{MP} and were displayed respectively on Fig. 2(b) and Fig. 2(c).

2.5. Definition of the spatial coherence for S-MMG

The spatial coherence of two S-MMGs was determined by using two different methods. This section will briefly characterize these two methods. First, the similarity in the frequency domain between two S-MMGs $l(t)$ and $m(t)$ at different locations along the longitudinal axis of the muscle was estimated from the magnitude square of their coherence function $C_{lm}(f)$, defined as

$$|C_{lm}(f)|^2 = \frac{|G_{lm}(f)|^2}{G_{II}(f)G_{mm}(f)} \quad (2)$$

where f is the frequency of interest, $G_{II}(f)$ (resp. $G_{mm}(f)$) is the power spectrum of the signal $l(t)$ (resp. $m(t)$), and $G_{lm}(f)$ is the cross power spectrum of those two signals (Challis and Kitney, 1991). The magnitude squared coherence between S-MMG signals $l(t)$ and $m(t)$ was estimated using the “mscohere” MATLAB® function (The signal pro-

cessing toolbox, 2007), and resulted in a value between 0 and 1, with 1 meaning perfectly similar signals.

For each test, the first and last 0.25 s were disregarded from the signal for quality control, due to potential fluctuations of the produced torque level at the beginning and the end of each recording. Hence the total signal duration used to calculate the coherence (2) between pairs of S-MMG signals was 9.5 s. The power spectrum and cross-spectrum of the S-MMG were estimated by segmenting the S-MMG time series in overlapping windows ($N = 1100$ points long with 50% overlap) and the number of samples for the fast Fourier transform operation was selected as 256 and was done in a 1100 points window. The confidence level cl of the coherence function is given by

$$cl = 1 - (\alpha)^{\frac{1}{L}} \quad (3)$$

where L is the number of windowed segments in the time domain of the signals. L is calculated by the effective signal duration multiplied by the sampling frequency of the recording ($Fe = 1$ kHz) divided by the window length ($N = 1100$ points) (Halliday et al., 1995). With $\alpha = 0.05$, (3) defines the degree of confidence as 95%.

$$L = \frac{(T)(Fe)}{N} = \frac{(9.5s)(1kHz)}{1100} = 8.6364 \quad (4)$$

Using (3) the confidence level was set to $cl \approx 0.32$ in this study, based on the selected parameters. Magnitude squared coherence values above this value of 0.32 can be determined to have significant coherence between the two signals. The frequency \hat{f} , beyond which the spatial coherence value drops below the significant level of 0.32 is described hereafter as the cut-off frequency.

Finally, at each contraction level (%MVC) the frequency-averaged coherence $|C_{lm}(f_c)|^2$ for varying center frequency f_c was defined as:

$$|C_{lm}(f_c)|^2 \simeq \int_{f_c-\Delta f}^{f_c+\Delta f} |C_{lm}(f)|^2 df \quad (5)$$

where $\Delta f = 2$ Hz. This frequency averaging over a 4 Hz frequency band yielded a more stable estimate of the magnitude square coherence values in the vicinity of the selected center frequency f_c .

Another method to calculate the similarity between two narrowband S-MMG signals $l(t)$ and $m(t)$ recorded at different locations uses the time-domain cross-correlation function $R_{lm}(\tau)$ defined as

$$R_{lm}(\tau) = \frac{\int_{-T/2}^{T/2} l(t)m(t+\tau)dt}{\sqrt{\int_{-T/2}^{T/2} l^2(t)dt \int_{-T/2}^{T/2} m^2(t)dt}} \quad (6)$$

In this study, the S-MMGs $l(t)$ and $m(t)$ were filtered with a second order Butterworth filter with a frequency band of $f_c \pm \Delta f$ with $\Delta f = 2$ Hz. The magnitude of the time-domain cross-correlation function was normalized between +1 and 0, where +1 indicates a perfect similarity between the two signals. Hence a measure of the spatial coherence of the narrowband S-MMGs $l(t)$ and $m(t)$ was also obtained from the peak values $X_{lm}(f_c)$ of the time-domain cross-correlation function (CCF):

$$X_{lm}(f_c) = |\max(R_{lm}(\tau))|^2 \quad (7)$$

It can be shown that the two metrics, $X_{lm}(f_c)$ and $|C_{lm}(f_c)|^2$ become approximately equal as the selected frequency band $2\Delta f$ reduces to zero (Gardner, 1992).

2.6. Statistical analysis

Statistical analysis was performed on signal to noise ratio, mean power frequency f_{MP} (1), S-MMG coherence $|C_{lm}(f_c)|^2$ (5), and S-MMG peak CCF $X_{lm}(f_c)$ (7). All of the data for each subject, for this

analysis, were averaged across the 3 trials. A one way analysis of variance (ANOVA) with repeated measure was used to test the main effect of contraction intensity on signal to noise ratio. An ANOVA with repeated measures was also used to test the main effect of contraction intensity on f_{MP} that was averaged across sensors at each contraction intensity. To determine the effect of frequency on coherence, the magnitude squared coherence value at 10 Hz intervals was averaged across sensor pairs, and contraction intensity was used in each sensor orientation. The main effect of frequency on coherence was tested with a one-way ANOVA with repeated measures for frequency. To test the main effect of sensor distance, contraction intensity, and sensor orientation direction on spatial coherence, the average spatial coherence centered at f_{MP} with 4 Hz bin was calculated. To test the effect of sensor distance, a one-way ANOVA with repeated measures for sensor distance was performed on spatial coherence values averaged across contraction intensity in each sensor orientation direction. Since the main effect of sensor distance was found in the longitudinal direction (as presented below), the data above $2\Delta y$ were removed in further statistical analyses to match data between sensor orientation directions. The effect of contraction intensity and sensor orientation direction was tested with a two-way ANOVA with repeated measures. An α level of 0.05 (where $(1 - \alpha)$ is the degree of confidence (Walpole et al., 2007)) was used for all statistical comparisons, and $P < 0.05$ and $P < 0.01$ are noted where appropriate (where the P value is a measure of the relative frequency or likelihood of occurrence of an event (Porkess, 1991)). In the figures, the error bars represent one standard deviation.

3. Results

3.1. Spatial coherence of S-MMGs

3.1.1. Signal-to-noise ratio and power spectrum density

An example of the power spectrum variations across frequency for increasing contraction level in one subject is shown in Fig. 2(a). In grouped data, the recorded S-MMG had a high signal to noise ratio that increased with contraction level ($P < 0.01$) (Fig. 2(b)). f_{MP} also increased with contraction level ($P < 0.01$) (Fig. 2(c)).

3.1.2. Examples for S-MMG coherence

The influence of contraction level, sensor separation distance, and sensor pair orientation (i.e., longitudinal vs. transverse) on S-MMG coherence (2) are illustrated in Fig. 3. Fig. 3(a) shows an example at 40% MVC that, for sensor pairs oriented along the longitudinal direction, the S-MMG coherence decreased for both increasing frequencies and increasing sensor separation distance. In contrast, the S-MMG coherence of sensor pairs oriented along the transverse direction was low across frequencies at 40% MVC (Fig. 3(b)). Similar results were observed for all other contraction levels. Fig. 3(c) and Fig. 3(d) illustrate the effect of contraction level on S-MMG coherence between two sensor pairs aligned either along the longitudinal or transverse direction but having a similar separation distance. The cut-off frequency \hat{f} for the threshold of significant coherence appeared to increase with contraction level in the longitudinal direction (Fig. 3(c)) but not in the transverse direction (Fig. 3(d)). When statistically analyzed across all sensor pairs in the longitudinal direction, the average cut-off frequency \hat{f} increased ($P < 0.01$) as contraction level increased. The cut-off frequencies were 40.43 ± 3.72 Hz, 54.86 ± 8.39 Hz and 64.87 ± 7.72 Hz, at 20% MVC, 40% MVC, and 60% MVC, respectively.

3.1.3. Effects of MMG frequency on S-MMG coherence

When using all the coherence data and considering only the main effect of frequency in each sensor pair orientation, the S-

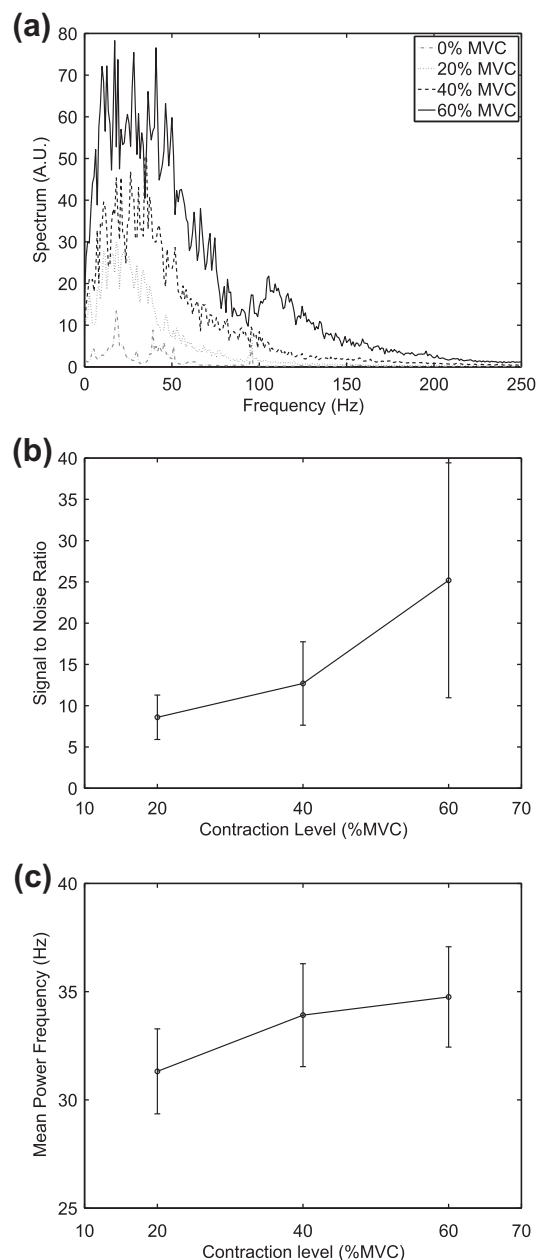


Fig. 2. (a) Example of S-MMG power spectrum for a subject measured on the central sensor (#8) for varying contraction level, (b) signal to noise ratio across all recorded signals as a function of contraction level across subjects, (c) mean power frequency (f_{MP}) of S-MMG as a function of contraction level averaged across subjects.

MMG coherence decreased with increasing frequency in both longitudinal ($P < 0.01$) (Fig. 4(a)) and transverse ($P < 0.05$) (Fig. 4(b)) directions. The cut-off frequency was higher ($P < 0.01$) for longitudinal sensor pairs (62.38 ± 4.54 Hz) than for transverse sensor pairs (31.70 ± 3.88 Hz).

3.1.4. Variation of S-MMG coherence and S-MMG peak cross correlation function (CCF) values

The S-MMG coherence (5) (Figs. 5(a,b)) and the S-MMG peak CCF (7) (Figs. 5(c,d)) between all sensor pairs at two frequency bands ($\frac{1}{3}f_{MP}$ and f_{MP}) are displayed in a checkerboard matrix representation in Fig. 5. The color bar in Fig. 5 denotes the level of spatial coherence, while the position of each individual box denotes which pair of sensors is under consideration (i.e., the extreme bottom

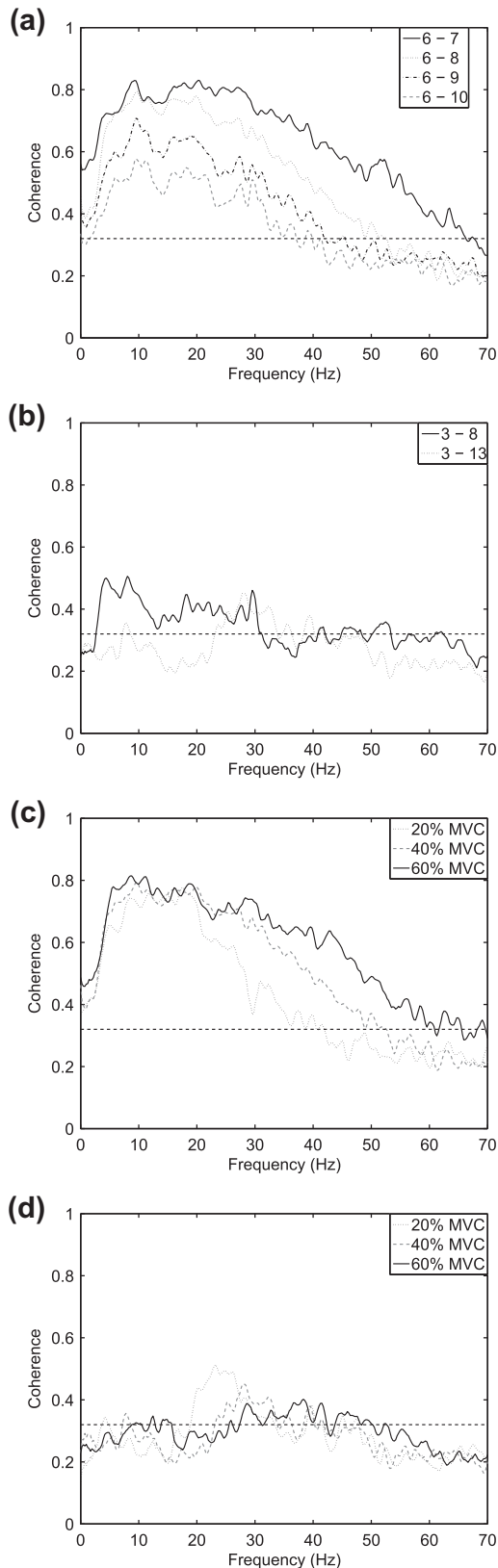


Fig. 3. The magnitude squared S-MMG coherence $|C_{im}(f)|^2$ averaged across subjects at the same contraction level (40 % MVC) for various separation distances between pairs of accelerometers located on (a) the central longitudinal sensor line and (b) the central transverse sensor line (see Fig. 1(c)). The magnitude squared S-MMG coherence $|C_{im}(f)|^2$ at a fixed sensor separation distance r between a pair of accelerometers located on (c) the center longitudinal sensor line (sensor pair 7 and 9, $r = 2\Delta y = 4.92 \pm 0.19$ cm) and (d) the center transverse sensor line (sensor pair 3 and 13, $r = 2\Delta x = 4$ cm) at each contraction level.

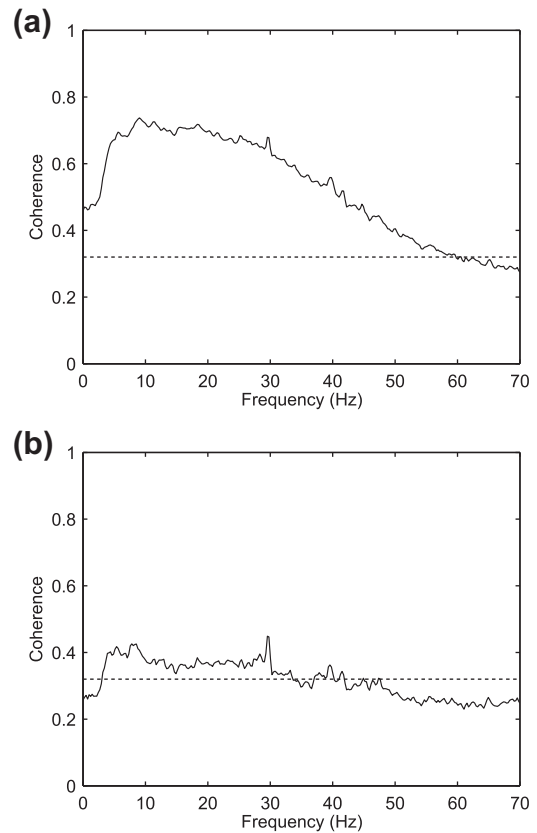


Fig. 4. The magnitude squared coherence averaged for sensor pairs oriented along (a) vertical grid lines (i.e., longitudinal direction) and (b) horizontal grid lines (i.e., transverse direction). The data were averaged across trials, contraction levels, and subjects.

right box gives the spatial coherence between sensors 1 and 15). On average, $\frac{1}{3}f_{MP}$ and f_{MP} were 11.11 ± 0.58 Hz and 33.33 ± 1.79 Hz, respectively (based on Fig. 2(c)).

These two center frequencies were used to investigate the difference in spatial coherence values due to the different physiological muscle activity at low ($f < 25$ Hz) and high ($f > 25$ Hz) frequencies Brown et al., 1982; Goldenberg et al., 1991; Orizio, 1993. For the frequency band centered on f_{MP} , significant spatial coherence values were obtained mainly between the set of five sensors located on the same vertical grid line (either medial, central or lateral, Fig. 1(c)) as evidenced by the 5×5 block diagonal pattern (delimited by black dashed lines) of this checkerboard matrix. For the frequency band centered at $\frac{1}{3}f_{MP}$, higher spatial coherence values were obtained also in the off diagonal 5×5 block (e.g., between sensors 6–10 and sensors 1–5, denoting the transverse direction). Because of the similarities between the values obtained using the two selected metrics, namely the S-MMG coherence (5) and the S-MMG peak CCF (7) (Figs. 5(a) and (5(c))), only the coherence values are reported hereafter.

3.1.5. Effects of sensor distance on S-MMG coherence

The S-MMG coherence decreased with increasing distance ($P < 0.01$) along the longitudinal direction for both frequency bands (Fig. 6(a)). When collapsed across sensor separation distances along the longitudinal direction, the S-MMG coherence centered at $\frac{1}{3}f_{MP}$ were higher ($P < 0.01$) compared with the one at f_{MP} . The pair-wise difference was significant ($P < 0.01$) at all sensor separation distances greater than Δy . In the transverse direction, the S-MMG coherence at $\frac{1}{3}f_{MP}$ were higher ($P < 0.05$) than the one centered at f_{MP} at $\Delta x = 2$ cm (Fig. 6(b)).

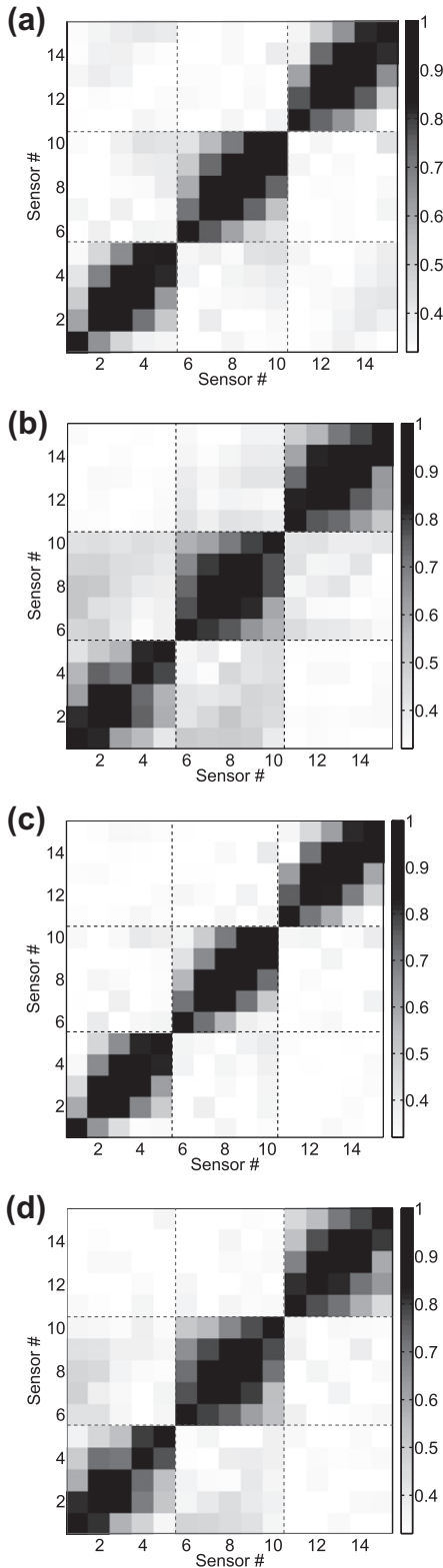


Fig. 5. Magnitude squared coherence values $|C_{im}(f_c)|^2$ (5) between all sensor pairs centered at (a) f_{MP} and (b) $\frac{1}{3}f_{MP}$. Normalized cross correlation peak values $X_{im}(f_c)$ (7) between all sensor pairs centered at (c) f_{MP} and (d) $\frac{1}{3}f_{MP}$. Data were averaged across trials, contraction levels, and subjects.

3.1.6. Effects of contraction level on S-MMG coherence

In the longitudinal direction, the S-MMG coherence increased as contraction level increased ($P < 0.01$) only for $f_c = f_{MP}$ (Fig. 7(a)). There was no effect of contraction level in the transverse direction

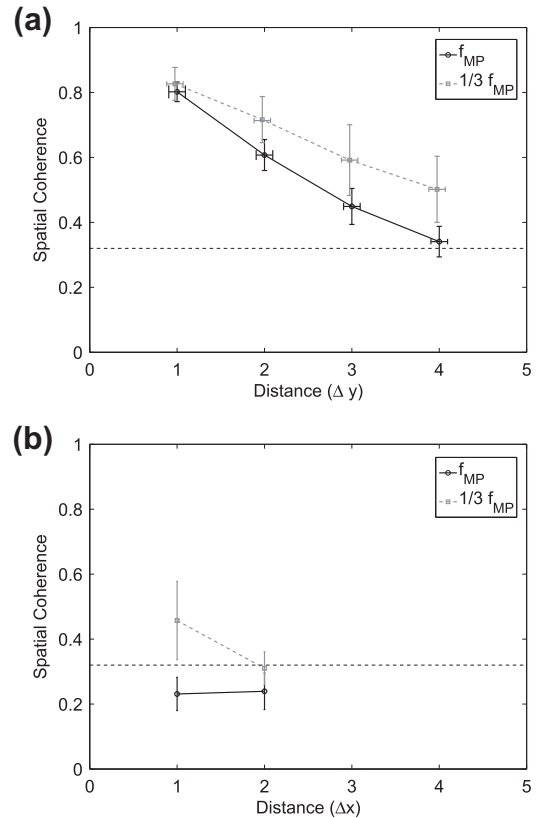


Fig. 6. Spatial coherence for 2 frequency bands in the (a) longitudinal and (b) transverse directions as a function of sensor distance. The spatial coherence values in a 4 Hz frequency band centered at f_{MP} and at $\frac{1}{3}f_{MP}$ were averaged for all longitudinal sensor pairs spaced apart by Δy to $4\Delta y$ ($2.1 \text{ cm} \leq \Delta y \leq 2.7 \text{ cm}$) and all transverse sensor pairs spaced apart by Δx to $2\Delta x$ ($\Delta x = 2.0 \text{ cm}$) across trials, contraction levels, and subjects. The sensor separation distance was averaged across sensors with a common separation distance along the (a) longitudinal and (b) transverse directions.

(Fig. 7(b)). Fig. 7 shows the main effect of contraction level on S-MMG coherence for longitudinal (Fig. 7(a)) and transverse (Fig. 7(b)) sensor orientation direction.

3.1.7. Effects of direction on S-MMG coherence and S-MMG peak CCF values

When focusing on the main effect of sensor pair orientation, the S-MMG coherence was greater in the longitudinal direction than in the transverse direction ($P < 0.01$) (Fig. 8(a)). Using the mathematically similar metric of the normalized cross correlation peak (7), the results were the same (Fig. 8(b)). The values were significantly greater ($P < 0.01$) in the frequency band centered at $\frac{1}{3}f_{MP}$ compared with the frequency band centered at f_{MP} for both metrics used.

4. Discussion

The initial analysis of the S-MMG data collected for this study confirmed that both the S-MMG mean power frequency (f_{MP}) and S-MMG signal's intensity increased with the contraction level of the biceps (see Fig. 2), in agreement with previous studies (Orizio, 1993; Orizio, 2005; Jaskolska et al., 2007). The main finding of this study is that the spatial coherence values of high frequency (i.e., close to the mean power frequency f_{MP}) S-MMG propagating between sensor pairs aligned along the biceps main axis (i.e., the longitudinal direction) was significantly higher than the spatial

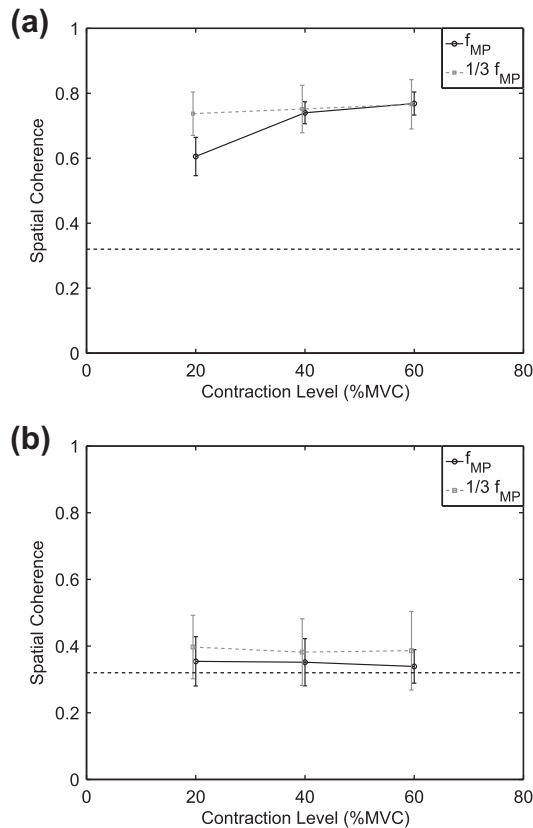


Fig. 7. The S-MMG coherence values $|C_{im}(f_c)|^2$ for 2 frequency bands in the (a) longitudinal and (b) transverse directions as a function of contraction level. Data in 4 Hz frequency band at f_{MP} or at $1/3 f_{MP}$ were averaged for all comparable sensor separation distances of Δy to $2\Delta y$ and Δx to $2\Delta x$ along the (a) longitudinal direction or (b) transverse direction across trials and subjects at each contraction level.

coherence values for sensor pairs oriented perpendicular to the muscle fibers (i.e., along the transverse direction) between the proximal and distal ends of the biceps (i.e., the longitudinal direction). In addition, the spatial coherence values at the lower frequency ($1/3 f_{MP}$) are on average higher than the values at the higher (f_{MP}) frequency. These main findings supported our hypotheses.

In the current study, three additional findings were obtained. First, the cut-off frequency of the S-MMG spatial coherence (i.e., the frequency beyond which the spatial coherence values dropped below the confidence level) significantly increased with contraction level, when considering longitudinal sensor pairs but not transverse sensor pairs. Second, the spatial coherence values of S-MMGs along the longitudinal direction decreased with increasing frequency and increasing sensor separation distance for both studied frequencies (f_{MP} and $1/3 f_{MP}$). Finally, the spatial coherence values between longitudinal sensor pairs increased with contraction level, but only for the frequency band centered at f_{MP} .

These findings can be related to the physiological origin of S-MMG. The local activation of the muscle fibers typically dominates the S-MMG generation mechanism in the higher frequency band (i.e., $f > 25$ Hz) (Orizio, 1993). Furthermore, the fast twitch fibers are more superficially located than slow twitch fibers in the biceps brachii muscle (Clamann, 1970). Hence, in the biceps brachii, the high frequency content of S-MMG, measured with skin-mounted sensors at the biceps brachii surface, is highly influenced by the physical characteristics and orientation of fast twitch fibers, especially at high contraction level (Orizio, 2005). The main finding of the current study demonstrated high coherence values of high frequencies S-MMG recorded along the biceps longitudinal axis.

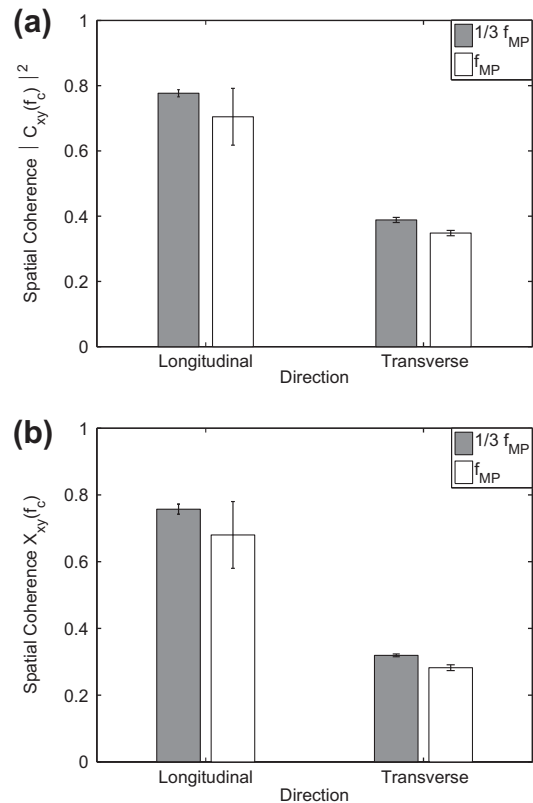


Fig. 8. Collapsed spatial coherence values across sensor separation distances and contraction levels in 2 frequency bands in each sensor pair orientation. (a) The magnitude square coherence $|C_{im}(f_c)|^2$ (5) and (b) the maximum normalized ross correlations $X_{im}(f_c)$ (7) are shown. The data were averaged for the 4 Hz frequency bands centered at $1/3 f_{MP}$ and f_{MP} .

These high coherence values indicate that a significant fraction of the muscles natural vibrations was recorded on all the selected longitudinal sensors locations. This finding is consistent with a previous preliminary study using the propagation velocity of coherent S-MMG along the biceps axis to infer muscle stiffness (Sabra and Archer, 2009). This likely results from the fusiform architectural organization of the biceps brachii muscle fibers (Winter, 1990): the longitudinal direction corresponds to the main orientation of the biceps brachii muscle's fibers and is thus likely more homogeneous than the transverse directions, thus favoring the propagation of natural muscle vibrations (Fung, 1988). Based on the first additional finding, it appears that the increase in discharge rate (associated with the increase in contraction level), is only paralleled by an increase in spatial coherence values of longitudinal sensor pairs and not transverse sensor pairs. Consequently, measurements of the spatial coherence of high-frequency S-MMG (i.e., $f > 25$ Hz), which are mainly generated by the a-synchronized muscle fiber activity, are likely to reflect the physiological architecture of the tested skeletal muscle. On the other hand, the spatial coherence values for low-frequency S-MMG ($f < 25$ Hz) appear to be significant along both the transverse and longitudinal directions. This likely occurs because low-frequency S-MMG are mainly produced by the synchronized activity of muscle fibers as a result of muscle tremor activity (Brown et al., 1982; Goldenberg et al., 1991) or movements of the whole limb due to motion artifacts, especially at higher contraction level. This may explain why an earlier study on S-MMGs for isometric contractions of the biceps brachii focusing on more energetic lower frequency S-MMG components (i.e., $f < 25$ Hz), concluded the S-MMGs propagate transversely, related

to a bending transverse modal resonances of the whole biceps (Ouamer et al., 1999).

Finally, the second and third additional findings may result from the influence of the muscle's mechanical properties and activation level on the propagation of the mechanical vibrations along the muscle. Two main factors are likely to influence the spatial coherence values of S-MMGs for this study. First, mechanical vibrations (e.g., as measured by S-MMGs) become rapidly attenuated when propagating in viscoelastic materials with high damping factors or viscosity (such as skeletal muscles) (Fung, 1988; Gennissou et al., 2010). Additionally, the influence of viscous effects on the propagation of mechanical vibrations increases with higher frequency and longer propagation distances. Thus, the propagation distance of such mechanical vibrations is limited by the viscous attenuation and decreases as the frequency content of the vibration increases. Consequently, the viscous attenuation of the muscle likely limits the sensor separation distance over which mechanical vibrations can propagate coherently between the skin-mounted accelerometers (as observed from the second additional finding), especially as S-MMG frequency increases. Hence, at the lower frequency band, the spatial coherence vs. distance, even in the transverse direction, shows a significant difference between the two sensor separation distances (Δx , $2\Delta x$ and Δy , $2\Delta y$). Second, a more homogeneous (or spatially uniform) propagation medium favors the undisturbed propagation of mechanical vibrations: spatial heterogeneities in mechanical properties destroy the relative phase relationships, and thus the resulting spatial coherence level, of propagating vibrations between spatially separated sensors (Gardner, 1992). For instance, the longitudinal direction is more mechanically homogeneous than the transverse directions (Fung, 1988). Additionally, the muscle's stiffness increases as the contraction level increases (Fung, 1988; Gennissou et al., 2010) thus increasing in turn the mechanical coupling (and homogeneity) between longitudinal sensor pairs. Consequently, the latter two effects likely cause the apparent increase in the spatial coherence values between longitudinal sensor pairs for the tested contraction levels: High frequency S-MMGs ($f > 25$ Hz), which are less influenced by synchronous muscle activity (muscle tremor or whole limb motion), likely propagates more coherently along the muscle fiber orientation (i.e., longitudinal direction) in a guided fashion as the biceps stiffens.

Overall the results of this study confirm that the multichannel skin-mounted sensor arrays measure spatial variations and coupling directionality of mechanical vibrations (as measured by S-MMG) over a contracting muscle in agreement with previous related studies (Sabra and Archer, 2009; Cescon et al., 2007; Madeleine et al., 2007; Farina et al., 2008; Cescon et al., 2008). However, the physical characteristics of these natural vibrations have very rarely been related to the actual mechanical properties of muscle soft tissues (Cole and Barry, 1994; Cescon et al., 2008). In particular, further studies on the spatial coherence of S-MMGs across various skeletal muscles could lead to objective techniques to measure the mechanical properties of skeletal muscles, such as muscle stiffness (Sabra et al., 2007; Sabra and Archer, 2009). To this end, the influence of muscular fatigue occurring during voluntary contractions on the spatial coherence of S-MMG requires further quantification. This study investigates the possibility of using S-MMG to determine mechanical properties of skeletal muscle, in addition to this, joint measurement of S-MMG and EMG can be investigated to determine electromechanical coupling as well as determining the localization of the source of mechanical vibrations. The spatial coherence of S-MMGs in humans with movement disorders (e.g., spasticity due to spinal cord injury or stroke) would be an important field of study for the quantification of muscle stiffness. Additionally, localization of the strength of coherence in S-MMGs between sensor pairs may provide further insights into

the potential mechanical compartmentalization that may be due to either localized mechanical properties or localized muscle activity (Segal, 1992) and possible dependency/independency between adjacent muscles or partitions (English et al., 1993; Shinohara, 2009; Shinohara et al., 2009).

5. Conclusions

The spatial coherence values of S-MMG at f_{MP} were significantly higher for longitudinal sensor pairs aligned along the biceps axis compared with transverse sensor pairs oriented across the biceps axis. This finding indicated that the mechanical coupling of coherent S-MMG appears to be highly directional along the longitudinal axis of the fusiform biceps muscle in higher frequency bands ($f > 25$ Hz), which suggests that there are propagating natural vibrations along the biceps longitudinal direction.

References

- The signal processing toolbox™: Magnitude squared coherence. The Mathworks™, Oct 2007. URL <<http://www.mathworks.com/access/helpdesk/help/toolbox/signal/index>>. <<http://www.mathworks.com/access/helpdesk/help/toolbox/signal/mscohere.html>>.
- Barry DT, Cole NM. Muscle sounds are emitted at the resonant frequencies of skeletal muscle. *IEEE Trans Bio-Med Eng* 1990;37:525–31.
- Beck TW, Housh TJ, Cramer JT, Weir JP, Johnson GO, Coburn JW, et al. Mechanomyographic amplitude and frequency responses during dynamic muscle actions: a comprehensive review. *Biomed Eng Online* 2005;4:1–27.
- Brown T, Rack P, Ross H. Different types of tremor in the human thumb. *J Physiol-Lond* 1982;332:113–23. ISSN 0022-3751.
- Cescon C, Farina D, Gobbo M, Merletti R, Orizio C. Effect of accelerometer location on mechanomyogram variables during voluntary, constant-force contractions in three human muscles. *Med Biol Eng Comput* 2004;42(1):121–7. ISSN 0140-0118.
- Cescon C, Madeleine P, Farina D. Longitudinal and transverse propagation of surface mechanomyographic waves generated by single motor unit activity. *Med Biol Eng Comput* 2008;46(9):871–7. ISSN 0140-0118.
- Cescon C, Madeleine P, Graven-Nielsen T, Merletti R, Farina D. Two-dimensional spatial distribution of surface mechanomyographical response to single motor unit activity. *J Neurosci Meth* 2007;159(1):19–25. ISSN 0165-0270.
- Cescon C, Nannucci L, Orizio C. A prototype of hybrid probe for surface EMG and MMG joint recordings. In: Proceedings of the XIV Congress ISEK, Vienna, Austria, 2002. p. 299–300.
- Challis R, Kitney R. Biomedical signal-processing 3 the power spectrum and coherence function. *Med Biol Eng Comput* 1991;29(3):225–41. ISSN 0140-0118.
- Clamann H. Activity of single motor units during isometric tension. *Neurology* 1970;20(3):254–60. ISSN 0028-3878.
- Cole N, Barry D. Muscle sounds frequencies of the frog are modulated by skeletal-muscle tension. *Biophys J* 1994;66(4):1104–14. ISSN 0006-3495.
- English A, Wolf S, Segal R. Compartmentalization of Muscles and Their Motor Nuclei - The Partitioning Hypothesis. *Phys Ther* 1993;73(12):857–67. ISSN 0031-9023.
- Farina D, Li X, Madeleine P. Motor unit acceleration maps and interference mechanomyographic distribution. *J Biomech* 2008;41(13):2843–9. ISSN 0021-9290.
- Fung Y. *Biomechanics: Mechanical Properties of Living Tissues*. 2 edition. New York: Springer-Verlag; 1988.
- Gardner WA. A unifying view of coherence in signal processing. *Signal Process* 1992;29(2):113–40. ISSN 0165-1684.
- Gennissou J-L, Deffieux T, Mace E, Montaldo G, Fink M, Tanter M. Viscoelastic and anisotropic mechanical properties of in vivo muscle tissue assessed by supersonic shear imaging. *Ultrasound Med Biol* 2010;36(5):789–801. ISSN 0301-5629.
- Goldenberg M, Yack H, Cerny F, Burton H. Acoustics myography as an indicator of force during sustained contractions of a small hand muscle. *J Appl Physiol* 1991;70(1):87–91. ISSN 8750-7587.
- Graaff KVD. *Human Anatomy*. 6 edition. New York: McGraw-Hill; 2002.
- Halliday D, Rosenberg J, Amjad A, Breeze P, Conway B, Farmer S. A framework for the analysis of mixed time series/point process data - theory and application to the study of physiological tremor, single motor unit discharges and electromyograms. *Progr Biophys Mol Biol* 1995;64(2-3):237–78. ISSN 0079-6107.
- Jaskolska A, Madeleine P, Jaskolski A, Kisiel-Sajewicz K, Arendt-Nielsen L. A comparison between mechanomyographic condenser microphone and accelerometer measurements during submaximal isometric, concentric and eccentric contractions. *J Electromyogr Kinesiol* 2007;17(3):336–47. ISSN 1050-6411.
- Kwatny E, Thomas DH, Kwatny HG. An application of signal processing techniques to the study of myoelectric signals. *IEEE Trans Biomed Eng* 1970;17:303–13.

- Madeleine P, Cescon C, Farina D. Spatial and force dependency of mechanomyographic signal features. *J Neurosci Meth* 2006;158(1):89–99. ISSN 0165-0270.
- Madeleine P, Toker K, Arendt-Nielsen L, Farina D. Heterogeneous mechanomyographic absolute activation of paraspinal muscles assessed by a two-dimensional array during short and sustained contractions. *J Biomech* 2007;40(12):2663–71. ISSN 0021-9290.
- Orizio C. Muscle sound - bases for the introduction of a mechanomyogram signal in muscle studies. *Crit Rev Biomed Eng* 1993;21(3):201–43. ISSN 0278-940X.
- Orizio C. Surface Mechanomyogram (Chapter 11 of *Electromyography: Physiology, Engineering, and Noninvasive Applications.*). Wiley-IEEE Press; 2005.
- Oster G, Jaffe JS. Low-frequency sounds from sustained contraction of human skeletal-muscle. *Biophys J* 1980;130:119–27.
- Ouamer M, Boiteux M, Petitjean M, Travens L, Sales A. Acoustic myography during voluntary isometric contraction reveals non-propagative lateral vibration. *J Biomech* 1999;32(12):1279–85. ISSN 0021-9290.
- Pappas G, Asakawa D, Delp S, Zajac F, Drace J. Nonuniform shortening in the biceps brachii during elbow flexion. *J Appl Physiol* 2002;92(6):2381–9. ISSN 8750-7587.
- Porkess R. *The HarperCollins Dictionary of Statistics*. New York: HarperCollinsPublishers, Inc.; 1991.
- Romano AJ, Abraham PB, Rossman PJ, Bucaro JA, Ehman RL. Determination and analysis of guided wave propagation using magnetic resonance elastography. *Magn Reson Med* 2005;54(4):893–900. ISSN 1522-2594. URL <http://www.doi.org/10.1002/mrm.20607>.
- Sabra KG, Archer A. Tomographic elastography of contracting skeletal muscles from their natural vibrations. *Appl Phys Lett* 2009;95(20). ISSN 0003-6951.
- Sabra KG, Conti S, Roux P, Kuperman W. Passive in vivo elastography from skeletal muscle noise. *Appl Phys Lett* 2007;90(19). ISSN 0003-6951.
- Segal R. Neuromuscular compartments in the human biceps brachii muscle. *Neurosci Lett* 1992;140(1):98–102. ISSN 0304-3940.
- Shinohara M. Muscle Activation Strategies in Multiple Muscle Systems. *Med Sci Sports Exer* 2009;41(1):181–3. ISSN 0195-9131.
- Shinohara M, Sogaard K. Mechanomyography for studying force fluctuations and muscle fatigue. *Exercise Sport Sci Rev* 2006;34:59–64.
- Shinohara M, Yoshitake Y, Kouzaki M. Alterations in Synergistic Muscle Activation Impact Fluctuations in Net Force. *Med Sci Sports Exer* 2009;41(1):191–7. ISSN 0195-9131.
- Walpole RE, Myers RH, Myers SL, Ye K. *Probability and statistics for engineers and scientists*. 8th ed. New Jersey: Pearson Prentice Hall, Upper Saddle River; 2007.
- Watakabe M, Mita K, Akataki K, Ito K. Reliability of the mechanomyogram detected with an accelerometer during voluntary contractions. *Med Biol Eng Comput* 2003;41(2):198–202. ISSN 0140-0118.
- Winter DA. *Biomechanics and motor control of human movement*. New York: John Wiley & Sons; 1990.



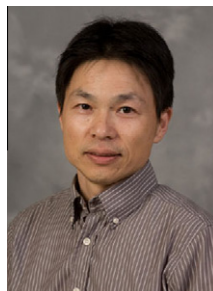
Akibi Archer received his BS in Mechanical Engineering in 2007 at the University of Florida, Gainesville, Florida and his MS in Mechanical Engineering in 2010 at the Georgia Institute of Technology, Atlanta, Georgia. He is currently pursuing his Ph.D., working in the Wave Physics Lab at the Georgia Institute of Technology, in the School of Mechanical Engineering.



Perry Atangcho was born in Cameroon in 1986. He received his BS in Biomedical Engineering from Georgia Institute of Technology in December 2010. He is currently pursuing a Masters in Quantitative and Computational Finance at Georgia Institute of Technology.



Karim Sabra received a MS degree from the University of Michigan and a M.Sc. degree from École National Supérieure de Techniques Avancées, France in 2000 and received his Ph.D. in Mechanical Engineering from the University of Michigan 2003. He began at Georgia Tech in 2007 as an Assistant Professor. Prior to this he was a Project Scientist at the Marine Physical Laboratory of the Scripps Institute of Oceanography at the University of California at San Diego.



Minoru Shinohara received the B.Ed., M.Ed., and Ph.D. degrees from University of Tokyo, Japan. In 2006, following faculty and research appointments at University of Tokyo, Pennsylvania State University, and University of Colorado at Boulder, he was appointed as Associate Professor of Applied Physiology at Georgia Institute of Technology. He is an Associate Editor of *Medicine and Science in Sports and Exercise* and an Editorial Board member of *Journal of Electromyography and Kinesiology* and *Journal of Applied Physiology*.